ACS APPLIED MATERIALS & INTERFACES

www.acsami.org

Research Article

Controlling Magnetization Vector Depth Profiles of $La_{0.7}Sr_{0.3}CoO_3$/$La_{0.7}Sr_{0.3}MnO_3$ Exchange Spring Bilayers via Interface Reconstruction

Alexander M. Kane,[#] I-Ting Chiu, Nolan J. Ahlm, Rajesh V. Chopdekar, Alpha T. N'Diaye, Elke Arenholz, Apurva Mehta, Valeria Lauter,[#] and Yayoi Takamura*[,#]

Cite This: *ACS Appl. Mater. Interfaces* 2020, 12, 45437−45443

Read Online

ACCESS | Metrics & More | Article Recommendations | Supporting Information

ABSTRACT: The $La_{0.7}Sr_{0.3}CoO_{3-\delta}$/$La_{0.7}Sr_{0.3}MnO_{3-\delta}$ (LSCO/LSMO) bilayer system is an ideal perovskite oxide platform for investigating interface reconstruction and its effect on their magnetic properties. Previous studies have shown that LSCO can separate into magnetic sublayers, which possess distinct trends as the total LSCO thickness increases. In this study, we used polarized neutron reflectometry to quantify changes in the magnetic and chemical depth profiles, and it confirms the formation of ∼12 Å-thick interfacial LSCO and LSMO layers, characterized by a decreased nuclear scattering length density compared to the bulk of the layers. This decrease is attributed to the combined effects of oxygen vacancy formation and interfacial charge transfer, which lead to magnetically active Co^{2+} ions with ionic radii larger than the Co^{3+}/Co^{4+} ions typically found in bulk LSCO or single-layer films. The interfacial magnetization values, as well as Co^{2+} ion and oxygen vacancy concentrations, depend strongly on the LSCO layer thickness. These results highlight the sensitive interplay of the cation valence states, oxygen vacancy concentration, and magnetization at interfaces in perovskite oxide multilayers, demonstrating the potential to tune their functional properties via careful design of their structure.

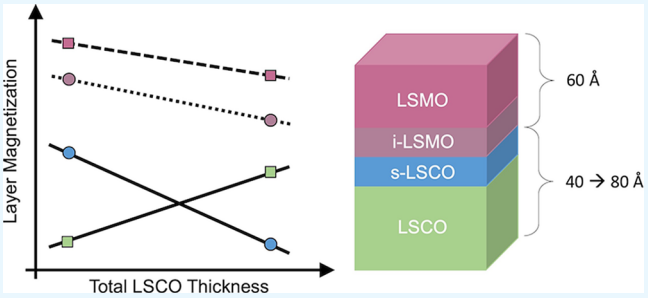

KEYWORDS: *magnetism, exchange bias, perovskites, thin films, charge transfer, interface reconstruction, polarized neutron reflectometry*

INTRODUCTION

Perovskite oxides have received significant interest for applications in next-generation magnetic and ferroelectric devices due to their tunable charge, spin, lattice, and orbital degrees of freedom that provide remarkable sensitivity to external stimuli.[1] In particular, interfaces in multilayers have been shown to drive charge transfer reactions and unexpected phenomena that are not observed in the constituent materials.[2−5] Exchange spring magnets, bilayers composed of hard/soft magnetic materials, have been studied intensely for their use as permanent magnets[6,7] and in heat-assisted magnetic recording devices.[8,9] Most exchange spring research has been focused on metal bilayers, but an all-oxide exchange spring could provide a degree of tunability absent in the purely metallic counterparts. One example is the perovskite exchange spring bilayer composed of $La_{0.7}Sr_{0.3}CoO_{3-\delta}$ and $La_{0.7}Sr_{0.3}MnO_{3-\delta}$ (LSCO/LSMO), hard and soft ferromagnetic (FM) layers, respectively. In this system, an interfacial layer characterized by magnetically active Co^{2+} ions (s-LSCO) couples to, and switches concurrently with, the soft LSMO layer.[10,11] Previous studies have suggested that for LSCO thicknesses greater than ∼50 Å, beneath the s-LSCO layer, the remaining LSCO layer maintains the expected Co^{3+}/Co^{4+} valence state and hard FM behavior of single-layer films (h-LSCO). The h-LSCO layer imposes a reversible exchange bias (EB) shift in the coupled soft layers in a direction opposite to the bias field. A detailed spectroscopy study as a function of LSCO layer thickness demonstrated that the Co^{2+} ion concentration is inversely related to the total LSCO thickness.[12] However, these prior studies were unable to quantitatively determine the interface layer magnetization and thickness, the role of oxygen vacancies, and whether magnetization reversal proceeds via a gradual unwinding as with metallic exchange springs or via domain nucleation within the soft layer.

To address these questions, we used polarized neutron reflectometry (PNR), which combines the depth sensitivity of thin-film reflectivity experiments with the magnetization-dependent scattering of polarized neutrons, as well as the capability to quantify changes in oxygen content from nuclear scattering that is typically difficult due to its low atomic mass.[13−16] Among a variety of magnetic systems, this technique has been used to map the chiral magnetic structures

Received: May 23, 2020
Accepted: August 27, 2020
Published: August 27, 2020

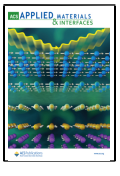

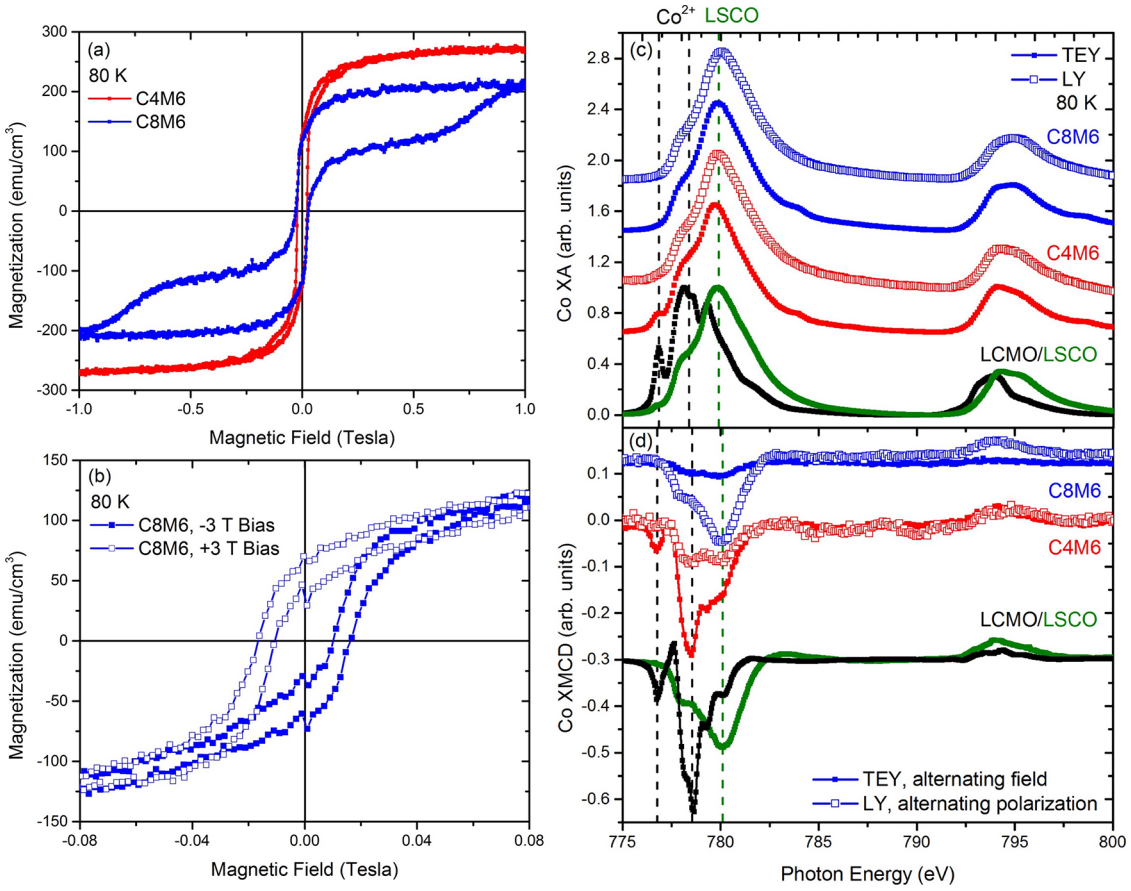

Figure 1. Bulk magnetization: (a) major hysteresis loops and (b) biased minor hysteresis loops. The minor hysteresis loops have been centered vertically to remove the shift due to the saturated h-LSCO layer not reversed by 0.1 T magnetic fields. (c) Co-XA and (d) Co-XMCD spectra; closed/open symbols correspond to TEY/LY detection. LY Co-XMCD spectra were collected with a fixed field and alternating circular polarization after field cooling in 0.3 T, while TEY Co-XMCD spectra were taken with ±0.3 T and fixed circular polarization. Black and green curves correspond to $Co^{2+}$and Co^{3+}/Co^{4+} reference spectra, respectively.

of metallic exchange spring multilayers including the SmCo/Fe,[17] $CoFe_2O_4/CoFe_{10}$,[18] Fe/Cr,[19] and $Fe_{55}Pt_{45}/Ni_{80}Fe_{20}$[20] systems. It has also attracted intense interest in the study of perovskite oxide thin films and multilayers, owing to their unusual magnetic behavior produced by interfacial electronic reconstruction. Hoffman et al. revealed that a noncollinear magnetic structure existed between successive LSMO layers in $(LaNiO_3)_n/(LSMO)_9$ superlattices (n is the number of unit cells), which they attributed to charge transfer at the $LaNiO_3$/LSMO interface and Ni^{2+} ions that couple to the LSMO layers.[21,22] Furthermore, in situ measurements of magnetic depth profiles in ion gel-gated $La_{0.5}Sr_{0.5}CoO_{3-\delta}$ films correlated a decrease in magnetization to gating-induced oxygen vacancy formation.[23] Gilbert et al. investigated oxygen vacancies introduced in Gd-capped LSCO films, which produced a spontaneous redox reaction at room temperature to form GdO_x and led to degraded magnetic properties and a topotactic phase transition to the $La_{0.7}Sr_{0.3}CoO_{2.5}$ brownmillerite structure.[24,25] These examples highlight the need of a depth-sensitive probe-like neutron reflectometry to help unravel emergent interfacial phenomena and nanoscale magnetic variations in systems similar to the LSCO/LSMO bilayers investigated here.

The PNR measurements were combined with bulk magnetometry and soft X-ray magnetic spectroscopy to quantitatively describe changes in the chemical and magnetic depth profiles in two LSCO/LSMO bilayers resulting from electronic reconstruction. Two bilayers with different LSCO layer thicknesses were chosen to investigate the two switching regimes indicated from previous studies of this system:[11] the single-phase magnetic reversal when the LSCO thickness is below ∼50 Å and the two-phase reversal exchange biased regime for thicker LSCO layers. The PNR measurements reveal that the charge transfer interfacial layers of ∼12 Å possess decreased nuclear scattering length density compared to the bulk of the layers on both sides of the LSCO/LSMO interface. These results explain that the magnetization of the s-LSCO sublayer depends strongly on the LSCO thickness due to changes in the Co^{2+} ion and oxygen vacancy concentrations.

EXPERIMENTAL SECTION

The LSCO/LSMO exchange spring bilayers were grown on (001)-oriented $(LaAlO_3)_{0.3}(Sr_2TaAlO_6)_{0.7}$ (LSAT) substrates by pulsed laser deposition. The designed LSCO layer thicknesses were 40 and 80 Å, each capped with 60 Å of LSMO, referred to as samples C4M6 and C8M6, respectively. Therefore, the bilayers investigated here bridge the critical LSCO thickness needed to observe EB from the h-LSCO layer. The bilayers were grown at a substrate temperature of 700 °C in 300 mtorr O_2 pressure, using a KrF (248 nm) excimer laser at 0.9 J/cm^2 fluence and 1 Hz repetition rate. The samples were cooled to room temperature in 300 torr O_2 to ensure proper oxygen content within the bilayer.

The structural properties of the films were characterized by X-ray reflectivity (XRR), high-resolution $\omega-2\theta$ scans, and reciprocal space

https://dx.doi.org/10.1021/acsami.0c09417
ACS Appl. Mater. Interfaces 2020, 12, 45437−45443

maps (RSMs) with a Bruker D8 Discover X-ray diffractometer using Cu Kα_1 X-rays. They were further characterized using resonant X-ray reflectivity (RXRR) measurements at beamline 2-1 of the Stanford Synchrotron Radiation Lightsource at SLAC National Accelerator Laboratory. RXRR profiles were measured at the Co and Mn K-edges and an off-resonance energy (8 keV). By tuning the resonance energies of the B-site ions, we improve the scattering length density (SLD) contrast between perovskite oxide layers of similar chemical density.[26] All three energies were fit simultaneously to one structural model using GenX reflectivity software,[27] where atomic scattering factors were selected as additional fit parameters to account for on-resonance variations in the SLD. A carbon surface layer was added to the sample model due to prolonged sample exposure to hard X-rays in air.

The bulk magnetic properties were investigated using a Quantum Design VersaLab physical properties measurement system. Minor hysteresis loops were measured to ±0.4 T after biasing the sample with ±3 T. Magnetization values were calculated based on the total layer thicknesses of the bilayers. The magnetic/electronic structure was probed using X-ray absorption and X-ray magnetic circular dichroism (XA/XMCD) spectroscopy at beamline 4.0.2 of the Advanced Light Source (ALS) at Lawrence Berkeley National Laboratory. To ensure the saturation of the h-LSCO layer, the samples were field-cooled in 0.3 T and XMCD measurements were taken with a fixed field of 0.3 T and alternating circular polarization of the X-rays. Two detection methods were used: total electron yield (TEY), which provides surface sensitive measurements of the top 4−10 nm of the sample,[28] and luminescence yield (LY), which probes the full thickness of the film stack.[29] Therefore, Co-TEY measurements primarily probe the s-LSCO layer at the LSCO/LSMO interface, while Co-LY measurements are well suited to probe the buried h-LSCO layer. All magnetic and spectroscopy measurements were performed at 80 K.

PNR measurements were performed at the Magnetism Reflectometer (Beamline 4A) of the Spallation Neutron Source (SNS) at Oak Ridge National Laboratory[30] using the time-of-flight method and a neutron wavelength band of 2−5 Å. Bilayer C4M6 was measured in a saturating field of 1.1 T, while bilayer C8M6 was field-cooled in −1.1 T to saturate all magnetic layers, followed by measurement in 0.2 and 1.1 T, corresponding to antiparallel and parallel alignments of the hard/soft magnetic layers, respectively. R^+ and R^- spin channels were measured, which correspond to initial up/down neutron polarization, respectively, and the data was co-refined simultaneously in GenX[27] with XRR data.

RESULTS AND DISCUSSION

RXRR data and fits for the three X-ray energies are shown in Figure S1 for both bilayers, and the fit parameters are given in Tables S1 and S2. Best fits were obtained using a structural model that separates both the LSMO and LSCO layers into two sublayers with an interface roughness of ≤5 Å, indicating that the bilayers possess smooth structural interfaces with minimal chemical intermixing. $\omega-2\theta$ scans (Figure S2) display clear thickness fringes indicating that the bilayers possess a high degree of structural coherence in the out-of-plane direction. Fitting was performed using Bruker Leptos software,[31] and fit parameters are listed in Table S3. The layer thicknesses are in reasonable agreement with the designed values, and both film layers are coherently strained to the LSAT substrate as demonstrated by the reciprocal space maps in Figure S3.

The bulk magnetic hysteresis loops of the two bilayers (Figure 1a) display the expected behavior for LSCO/LSMO bilayers with LSCO layer thicknesses, that bridge the critical LSCO thickness for EB from the h-LSCO layer.[10−12] Bilayer C4M6 displays a single, sharp transition due to the magnetic coupling of the s-LSCO and LSMO layers, while bilayer C8M6 shows two magnetic transitions from the h-LSCO layer and the coupled soft layers. As a result, bilayer C8M6 displays an EB shift (Figure 1b) in the biased minor loops characteristic of exchange spring systems. The minor hysteresis loops have been centered vertically to remove the shift due to the saturated h-LSCO layer not reversed by 0.1 T magnetic fields.

Further insight into the magnetic behavior can be obtained from the Co-XA/XMCD spectra for the bilayers (Figure 1c,d with the reference spectra for Co^{2+} ions (La_2CoMnO_6 (LCMO)) and Co^{3+}/Co^{4+} ions (LSCO) included). While the differences in the shapes of the XA spectra between bilayers and comparing TEY and LY detection modes are subtle, notable differences exist in the XMCD spectra. For bilayer C4M6, a strong XMCD signal closely resembling the Co^{2+} reference spectrum is observed only for the TEY detection mode, confirming the presence of magnetically active Co^{2+} ions in the interfacial s-LSCO layer. The signature of Co^{2+} ions is also present in the TEY XA spectrum (features indicated by the vertical black dashed lines), while the corresponding LY XA spectrum is dominated by signatures of mixed Co^{3+}/Co^{4+} ions indicating that a weakly magnetic LSCO layer lies at the LSAT substrate interface. In contrast, the dominant XMCD signal for bilayer C8M6 is observed with the LY detection mode with characteristics dominated by mixed Co^{3+}/Co^{4+} ions of the h-LSCO layer. The TEY data exhibits an 85% decrease in XMCD peak intensity compared to the LY data and has nearly equal contributions from Co^{2+} and Co^{3+}/Co^{4+} type FM ordering. A slight shift of the main Co L_3 peak to lower energy in the TEY spectrum compared to the LY spectrum corroborates the presence of Co^{2+} ions at the LSCO/LSMO interface. Therefore, the magnetization of the s-LSCO layer decreases as the LSCO thickness increases due to the presence of the h-LSCO layer.[12]

The Mn spectra (Figure S4) resemble that for single-layer LSMO films for both bilayers. The main Mn L_3 peak in the LY spectra is shifted to slightly higher photon energies, indicative of a higher Mn^{4+}-to-Mn^{3+} ratio and consistent with charge transfer at the LSCO/LSMO interface.[10] The TEY XMCD peak intensity is 20% smaller than the LY data, likely due to a surface layer of reduced magnetization commonly observed in LSMO films.[32−36]

To clarify the relationship between total LSCO thickness, its constituent sublayer thicknesses and magnetization, and oxygen content, we next address the PNR data. Figure 2a plots this data for bilayer C4M6, where the splitting between the two spin channels indicates FM order. The best fits consisted of a model with two LSCO layers: the main layer at the substrate interface and the s-LSCO layer; and three LSMO layers: the interface layer with increased Mn^{4+} concentration, the main LSMO layer, and the surface layer of reduced magnetization.[32,33] The nuclear SLD from this fit (Figure 2b) indicates the formation of thin layers (12 Å or three unit cells) with a decrease in the nuclear SLD on either side of the LSCO/LSMO interface, 3.9 and 3.3% decreases for interface LSCO and LSMO layers, respectively. The densities of the main layers are consistent with the theoretical density. The thicknesses of these interface layers are consistent with that reported for charge transfer layers at oxide interfaces.[2,37] The reduced density likely results from the large ionic radius of Co^{2+} ions compared to Co^{3+}/Co^{4+} ions (18−32% larger for high-spin-state configurations)[38,39] and possibly the presence of oxygen vacancies.[40−42] Attributing this density loss solely to oxygen vacancies places upper bounds of oxygen non-

https://dx.doi.org/10.1021/acsami.0c09417
ACS Appl. Mater. Interfaces 2020, 12, 45437−45443

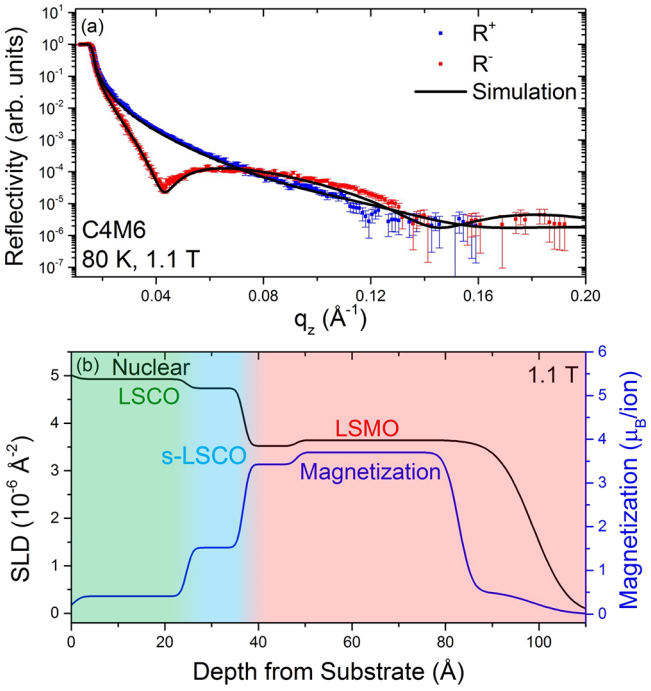

Figure 2. (a) Simultaneous PNR fits at 1.1 T and (b) nuclear SLD and magnetization profiles for bilayer C4M6.

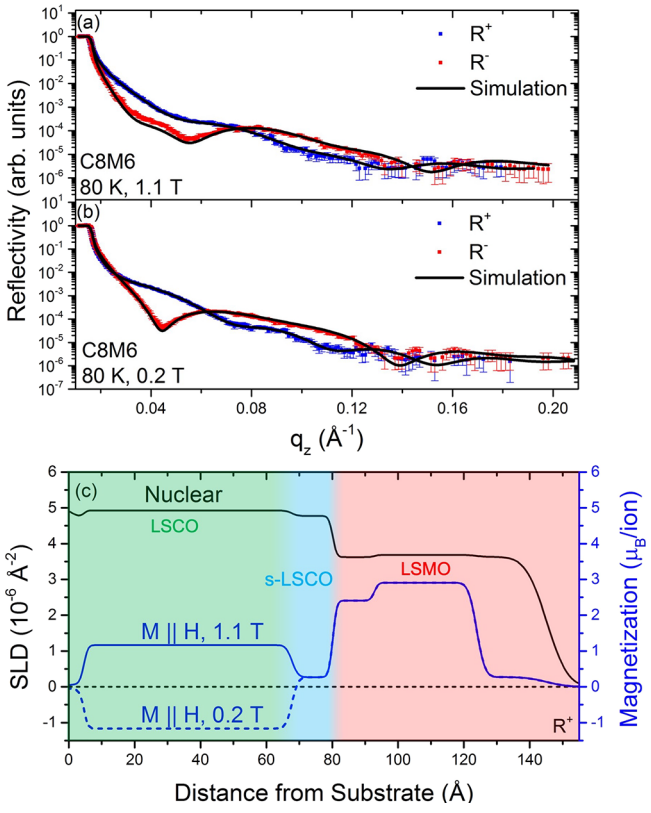

Figure 3. PNR data and fits for bilayer C8M6 at (a) 1.1 and (b) 0.2 T after an initial field cooling in −1.1 T. (c) Nuclear SLD and magnetization depth profiles.

stoichiometry at the interface at $\delta = 0.20 \pm 0.01$ for the LSCO and LSMO interface layers.[43] To confirm the sensitivity of the PNR model to the decrease in density for the interfacial layers, alternative fits are presented in Figures S5 and S6 for bilayer C4M6, each of which provides an inferior fit to the measured data. The corresponding sample magnetization indicates that the main LSCO layer retains a small magnetic moment (0.4 μ_B/Co ion or 66 emu/cm^3) compared to ∼0.9 μ_B/Co ion (150 emu/cm^3) for bulk LSCO,[44] while the s-LSCO layer has a much larger moment of 1.46 μ_B/Co ion (240 emu/cm^3). The magnetizations of the interface, main, and surface LSMO sublayers are 3.4 (538 emu/cm^3), 3.7 (586 emu/cm^3), and 0.52 μ_B/Mn ion (80 emu/cm^3), respectively, where the magnetization of the main layer is consistent with bulk values.[45] By comparing the magnetization values obtained from the PNR fits to the bulk magnetization data, described in greater detail in the Supporting Information, we estimate the individual layer magnetization values to be within ±20% of the neutron fit values, and the magnetization trends are consistent across all measurement techniques.

While bilayer C4M6 exhibited an LSCO interface layer with magnetization larger than bulk values, the PNR data and SLD profiles for bilayer C8M6 shown in Figure 3 exhibit the opposite behavior. Best fits were obtained using a similar model to bilayer C4M6 with an additional 4 Å nonmagnetic LSCO layer at the LSAT/LSCO interface[46] such that the LSMO and LSCO layers are both broken up into three sublayers. The LSCO and LSMO interface layers maintain a thickness of ∼12 Å with 3.1 and 1.6% nuclear SLD reductions for LSCO and LSMO, respectively. These densities correspond to upper bounds on oxygen nonstoichiometry of $\delta = 0.09 \pm 0.01$. A fit with fixed nSLD for all LSCO layers is presented in Figure S7, which shows larger deviation from the measured data compared to the fit with decreased density for the interfacial layers. The s-LSCO and h-LSCO layers have magnetizations of 0.29 and 1.16 μ_B/Co ion, respectively. The PNR fits for both bilayers also indicate the formation of an LSMO interface layer with decreased density. Unlike the Co^{2+} rich s-LSCO layer, the oxygen vacancies and charge transfer model produce counteracting effects on the Mn valence state in the LSMO layer; oxygen vacancies produce excess negative charge and thus a greater proportion of Mn^{3+} ions, while interfacial charge transfer between Co and Mn ions favors the formation of Mn^{4+} ions. The Mn XA spectra for the bilayers are consistent with these counteracting mechanisms as they show minimal deviation from an LSMO thin film.

In comparison to bilayer C4M6, the magnetization of the s-LSCO layer is significantly decreased, while that of the h-LSCO layer is enhanced, in agreement with the TEY/LY Co-XMCD signals for this bilayer. The magnetizations of the interface, main, and surface LSMO sublayers are 2.41, 2.91, and 0.27 μ_B/Mn ion, in reasonable agreement with those of bilayer C4M6. The difference in LSMO magnetization compared to C4M6 is likely attributed to an increase in Mn^{4+} ion concentration, which is expected to decrease the magnetization, an assertion supported by the Mn spectroscopy data in Figure S4. The as-designed LSMO is near the optimal doping limit for maximized magnetization and T_C,[47] and an increase in the Mn^{4+}-to-Mn^{3+} ratio effectively shifts the LSMO to higher Sr doping and leaves fewer 3d electrons to contribute to the magnetization. Furthermore, the magnetization profile indicates the antiparallel alignment of the h-LSCO and s-LSCO/LSMO layers at 0.2 T, with negative magnetization within the h-LSCO layer and no component of the magnetization perpendicular to the field direction. Therefore, magnetization reversal is likely driven by domain nucleation in the LSMO layer parallel to the magnetic field, which switches

https://dx.doi.org/10.1021/acsami.0c09417
ACS Appl. Mater. Interfaces 2020, 12, 45437−45443

the s-LSCO layer through interfacial coupling, rather than through a helical magnetic structure at the magnetic interface.

The magnetization depth profiles obtained from PNR measurements provide further information for our interface model of the LSCO thickness dependence of the magnetic behavior of LSCO/LSMO bilayers.[12] According to this model, the LSCO and LSMO layers break up into multiple sublayers with differing density, electronic structure, and magnetic properties. Charge transfer occurs across the LSCO/LSMO interface forming two interface layers of ∼12 Å thickness with increased Co^{2+} and Mn^{4+} ion concentrations, respectively, and with reduced densities compared to bulk values. Within the resolution of our measurements, the thickness of the interface layers is independent of LSCO thickness. On the LSMO side of the bilayer, the interfacial LSMO sublayer has suppressed magnetization, consistent with oxygen-deficient LSMO and an increase in the Mn^{4+}/Mn^{3+} ratio,[35,48,49] while the main and surface LSMO sublayers behave as expected for LSMO thin films.[32−36]

However, the behavior is more complex on the LSCO side of the bilayer. The s-LSCO layer is characterized by magnetically active Co^{2+} ions, which couple to the soft LSMO layer. As the LSCO layer thickness increases, the Co^{2+} ion concentration and XMCD contribution in the s-LSCO layer decrease, leading to a decrease in the s-LSCO magnetization, while the h-LSCO layer coercivity and magnetization gradually increase. As a result, a critical LSCO thickness of ∼50 Å exists, above which a distinct h-LSCO layer forms and which imposes a reversible EB shift in the coupled soft layers. Below the critical thickness, the s-LSCO layer is dominated by the magnetically active Co^{2+} ions leading to a large magnetization (1.46 μ_B/Co ion) and reduced density due to the relative $Co^{2+}/Co^{3+}/Co^{4+}$ ionic radii. In contrast, above the critical thickness, the Co^{3+}/Co^{4+} ions that replace Co^{2+} ions in the s-LSCO layer do not contribute significantly to its magnetization despite a valence state closely resembling that of bulk LSCO, which might suggest a bulk-like moment. We believe that this is due to the limited number of Co^{2+} ions, which disrupt the double exchange mechanism between Co^{3+} and Co^{4+} ions. The resulting s-LSCO magnetization lies below that of bulk LSCO, suggesting that the reduced density in this case occurs more due to oxygen vacancies at the interface, as the larger Co^{2+} ions comprise a much smaller percentage of interface Co ions. It should be noted that the small lattice mismatch between LSCO and LSAT (0.61% tensile strain) is expected to limit the driving force for the formation of ordered oxygen vacancies observed in cobaltite thin films,[50] such that we do not expect to form a significant amount of brownmillerite phase within the cobaltite layer.

CONCLUSIONS

In summary, we present a comprehensive interface model to explain the LSCO thickness dependence of the magnetic behavior of LSCO/LSMO bilayers. We determine that the length scale of electronic reconstruction in the form of charge transfer extends ∼12 Å from either side of the LSCO/LSMO interface. These interface layers are characterized by reduced density and increased Co^{2+} and Mn^{4+} ion concentrations compared to the bulk of the layers. The magnetization values of the LSCO sublayers depend strongly on the LSCO thickness: the s-LSCO magnetization decreases from 1.46 to 0.30 μ_B/Co ion for LSCO thicknesses of 40 and 80 Å, respectively, while the h-LSCO magnetization increases from 0.4 to 1.16 μ_B/Co ion, with a corresponding increase in coercivity. These trends result from a gradual decrease in the concentration of magnetically active Co^{2+} ions in the s-LSCO layer, as well as the presence of oxygen vacancies. As a result, a critical thickness of ∼50 Å exists, above which the h-LSCO layer forms and which can impose EB to the coupled s-LSCO/LSMO soft layers. These results highlight the interplay of charge transfer and oxygen stoichiometry in altering the magnetic profiles of perovskite oxide multilayers and provide a route to tune their functional properties via careful design of their structures.

ASSOCIATED CONTENT

Supporting Information

The Supporting Information is available free of charge at https://pubs.acs.org/doi/10.1021/acsami.0c09417.

Structural characterization, Mn spectroscopy data, and alternative polarized neutron reflectivity models (PDF)

AUTHOR INFORMATION

Corresponding Author

Yayoi Takamura − *Department of Materials Science and Engineering, University of California, Davis, Davis, California 95616, United States*; Email: ytakamura@ucdavis.edu

Authors

Alexander M. Kane − *Department of Materials Science and Engineering, University of California, Davis, Davis, California 95616, United States*; orcid.org/0000-0003-0864-724X

I-Ting Chiu − *Department of Chemical Engineering, University of California, Davis, Davis, California 95616, United States*

Nolan J. Ahlm − *Department of Materials Science and Engineering, University of California, Davis, Davis, California 95616, United States*

Rajesh V. Chopdekar − *Department of Materials Science and Engineering, University of California, Davis, Davis, California 95616, United States; Advanced Light Source, Lawrence Berkeley National Laboratory, Berkeley, California 94720, United States*; orcid.org/0000-0001-6727-6501

Alpha T. N'Diaye − *Advanced Light Source, Lawrence Berkeley National Laboratory, Berkeley, California 94720, United States*

Elke Arenholz − *Advanced Light Source, Lawrence Berkeley National Laboratory, Berkeley, California 94720, United States; Cornell High Energy Synchrotron Source, Cornell University, Ithaca, New York 14853, United States*

Apurva Mehta − *Stanford Synchrotron Radiation Lightsource, SLAC National Accelerator Laboratory, Menlo Park, California 94025, United States*; orcid.org/0000-0003-0870-6932

Valeria Lauter − *Neutron Scattering Division, Neutron Sciences Directorate, Oak Ridge National Laboratory, Oak Ridge, Tennessee 37830, United States*

Complete contact information is available at: https://pubs.acs.org/10.1021/acsami.0c09417

Author Contributions

#A.M.K., V.L., and Y.T. contributed equally. The manuscript was written through contributions of all authors. All authors have given approval to the final version of the manuscript.

Funding

Financial support for this project was provided by the University of California, Multicampus Research Programs and Initiatives grant MR-15-328528, National Science

Foundation grant DMR - 1745450, and the U.S. Department of Energy (DOE), Office of Science, Office of Workforce Development for Teachers and Scientists, Office of Science Graduate Student Research (SCGSR) program. The SCGSR program is administered by the Oak Ridge Institute for Science and Education (ORISE) for the DOE. ORISE is managed by Oak Ridge Associated Universities under contract number DE-SC0014664. This research used resources of the ALS, which is a DOE Office of Science User Facility under contract No. DE-AC02-05CH1123. Use of SSRL, SLAC National Accelerator Laboratory, is supported by the U.S. DOE, Office of Science, Office of Basic Energy Sciences under Contract No. DE-AC02-76SF00515. The research performed at ORNL's Spallation Neutron Source was sponsored by the Scientific User Facilities Division, Office of Basic Energy Sciences, U.S. Department of Energy.

Notes

The authors declare no competing financial interest.

REFERENCES

(1) Dagotto, E.; Hotta, T.; Moreo, A. Colossal Magnetoresistant Materials: The Key Role of Phase Separation. *Phys. Rep.* **2001**, *344*, 1−153.

(2) Ohtomo, A.; Muller, D. A.; Grazul, J. L.; Hwang, H. Y. Artificial Charge-Modulationin Atomic-Scale Perovskite Titanate Superlattices. *Nature* **2002**, *419*, 378−380.

(3) Ohtomo, A.; Hwang, H. Y. A High-Mobility Electron Gas at the $LaAlO_3/SrTiO_3$ Heterointerface. *Nature* **2004**, *427*, 423−426.

(4) Hwang, H. Y.; Iwasa, Y.; Kawasaki, M.; Keimer, B.; Nagaosa, N.; Tokura, Y. Emergent Phenomena at Oxide Interfaces. *Nat. Mater.* **2012**, *11*, 103−113.

(5) Zubko, P.; Gariglio, S.; Gabay, M.; Ghosez, P.; Triscone, J.-M. Interface Physics in Complex Oxide Heterostructures. *Annu. Rev. Condens. Matter Phys.* **2011**, *2*, 141−165.

(6) Fullerton, E. E.; Jiang, J. S.; Grimsditch, M.; Sowers, C. H.; Bader, S. D. Exchange-Spring Behavior in Epitaxial Hard/Soft Magnetic Bilayers. *Phys. Rev. B* **1998**, *58*, 193−12200.

(7) Fullerton, E. E.; Jiang, J. S.; Bader, S. D. Hard/Soft Magnetic Heterostructures: Model Exchange-Spring Magnets. *J. Magn. Magn. Mater.* **1999**, *200*, 392−404.

(8) Thiele, J.-U.; Maat, S.; Fullerton, E. E. FeRh/FePt Exchange Spring Films for Thermally Assisted Magnetic Recording Media. *Appl. Phys. Lett.* **2003**, *82*, 2859−2861.

(9) Thiele, J.-U.; Maat, S.; Robertson, J. L.; Fullerton, E. E. Magnetic and Structural Properties of FePt−FeRh Exchange Spring Films for Thermally Assisted Magnetic Recording Media. *IEEE Trans. Magn.* **2004**, *40*, 2537−2542.

(10) Li, B.; Chopdekar, R. V.; Arenholz, E.; Mehta, A.; Takamura, Y. Unconventional Switching Behavior in $La_{0.7}Sr_{0.3}MnO_3/La_{0.7}Sr_{0.3}CoO_3$ Exchange-Spring Bilayers. *Appl. Phys. Lett.* **2014**, *105*, 202401.

(11) Li, B.; Chopdekar, R. V.; N'Diaye, A. T.; Mehta, A.; Byers, J. P.; Browning, N. D.; Arenholz, E.; Takamura, Y. Tuning Interfacial Exchange Interactions via Electronic Reconstruction in Transition-Metal Oxide Heterostructures. *Appl. Phys. Lett.* **2016**, *109*, 152401.

(12) Kane, A. M.; Chopdekar, R. V.; N'Diaye, A. T.; Scholl, A.; Arenholz, E.; Mehta, A.; Takamura, Y. Decoupling Exchange Bias and Coercivity Enhancement in a Perovskite Oxide Exchange Spring Bilayer. *Phys. Rev. Mater.* **2019**, *3*, No. 014413.

(13) Lauter-Pasyuk, V. Neutron Grazing Incidence Techniques for Nano-Science. *Collect. SFN* **2007**, *7*, 221−240.

(14) Blundell, S. J.; Bland, J. A. C. Polarized Neutron Reflection as a Probe of Magnetic Films and Multilayers. *Phys. Rev. B* **1992**, *46*, 3391−3400.

(15) Toperverg, B. P. Polarized Neutron Reflectometry of Magnetic Nanostructures. *Phys. Metals Metallogr.* **2015**, *116*, 1337−1375.

(16) Ankner, J. F.; Felcher, G. P. Polarized-Neutron Reflectometry. *J. Magn. Magn. Mater.* **1999**, *200*, 741−754.

(17) Liu, Y.; te Velthuis, S. G. E.; Jiang, J. S.; Choi, Y.; Bader, S. D.; Parizzi, A. A.; Ambaye, H.; Lauter, V. Magnetic Structure in Fe/Sm-Co Exchange Spring Bilayers with Intermixed Interfaces. *Phys. Rev. B* **2011**, *83*, 174418.

(18) O'Donovan, K. V.; Borchers, J. A.; Maat, S.; Carey, M. J.; Gurney, B. A. Neutron Reflectivity on $CoFe_2O_4$ Exchange Springs for Spin Valve Applications. *J. Appl. Phys.* **2004**, *95*, 7507−7509.

(19) Lauter-Pasyuk, V.; Lauter, H. J.; Toperverg, B.; Nikonov, O.; Kravtsov, E.; Romashev, L.; Ustinov, V. Magnetic Neutron Off-Specular Scattering for the Direct Determination of the Coupling Angle in Exchange-Coupled Multilayers. *J. Magn. Magn. Mater.* **2001**, *226-230*, 1694.

(20) O'Donovan, K. V.; Borchers, J. A.; Majkrzak, C. F.; Hellwig, O.; Fullerton, E. E. Pinpointing Chiral Structures with Front-Back Polarized Neutron Reflectometry. *Phys. Rev. Lett.* **2002**, *88*, No. 067201.

(21) Hoffman, J. D.; Kirby, B. J.; Kwon, J.; Fabbris, G.; Meyers, D.; Freeland, J. W.; Martin, I.; Heinonen, O. G.; Steadman, P.; Zhou, H.; Schlepütz, C. M.; Dean, M. P. M.; te Velthuis, S. G. E.; Zuo, J.-M.; Bhattacharya, A. Oscillatory Noncollinear Magnetism Induced by Interfacial Charge Transfer in Superlattices Composed of Metallic Oxides. *Phys. Rev. X* **2016**, *6*, No. 041038.

(22) Hoffman, J. D.; Wu, S. M.; Kirby, B. J.; Bhattacharya, A. Tunable Noncollinear Antiferromagnetic Resistive Memory through Oxide Superlattice Design. *Phys. Rev. Appl.* **2018**, *9*, No. 044041.

(23) Walter, J.; Yu, G.; Yu, B.; Grutter, A.; Kirby, B.; Borchers, J.; Zhang, Z.; Zhou, H.; Birol, T.; Greven, M.; Leighton, C. Ion-Gel-Gating-Induced Oxygen Vacancy Formation in Epitaxial $La_{0.5}Sr_{0.5}CoO_{3-\delta}$ Films from *in Operando* x-Ray and Neutron Scattering. *Phys. Rev. Mater.* **2017**, *1*, No. 071403.

(24) Gilbert, D. A.; Grutter, A. J.; Murray, P. D.; Chopdekar, R. V.; Kane, A. M.; Ionin, A. L.; Lee, M. S.; Spurgeon, S. R.; Kirby, B. J.; Maranville, B. B.; N'Diaye, A. T.; Mehta, A.; Arenholz, E.; Liu, K.; Takamura, Y.; Borchers, J. A. Ionic Tuning of Cobaltites at the Nanoscale. *Phys. Rev. Mater.* **2018**, *2*, 104402.

(25) Rippy, G.; Trinh, L.; Kane, A. M.; Ionin, A. L.; Lee, M. S.; Chopdekar, R. V.; Christiansen-Salameh, J. M.; Gilbert, D. A.; Grutter, A. J.; Murray, P. D.; Holt, M. V.; Cai, Z.; Liu, K.; Takamura, Y.; Kukreja, R. X-Ray Nanodiffraction Studies of Ionically Controlled Nanoscale Phase Separation in Cobaltites. *Phys. Rev. Mater.* **2019**, *3*, No. 082001.

(26) Kemik, N.; Gu, M.; Yang, F.; Chang, C.-Y.; Song, Y.; Bibee, M.; Mehta, A.; Biegalski, M. D.; Christen, H. M.; Browning, N. D.; Takamura, Y. Resonant X-Ray Reflectivity Study of Perovskite Oxide Superlattices. *Appl. Phys. Lett.* **2011**, *99*, 201908.

(27) Björck, M.; Andersson, G. *GenX* : An Extensible X-Ray Reflectivity Refinement Program Utilizing Differential Evolution. *J. Appl. Crystallogr.* **2007**, *40*, 1174−1178.

(28) Lee, J.-S.; Arena, D. A.; Yu, P.; Nelson, C. S.; Fan, R.; Kinane, C. J.; Langridge, S.; Rossell, M. D.; Ramesh, R.; Kao, C.-C. Hidden Magnetic Configuration in Epitaxial La_{1-x} Sr_x MnO_3 Films. *Phys. Rev. Lett.* **2010**, *105*, 257204.

(29) Bianconi, A.; Jackson, D.; Monahan, K. Intrinsic Luminescence Excitation Spectrum and Extended X-Ray Absorption Fine Structure above the K Edge in CaF_2. *Phys. Rev. B* **1978**, *17*, 2021−2024.

(30) Lauter, V.; Ambaye, H.; Goyette, R.; Lee, W.-T. H.; Parizzi, A. Highlights from the Magnetism Reflectometer at the SNS. *Phys. B* **2009**, *404*, 2543−2546.

(31) *Leptos Manual*; Bruker AXS, W: 2005.

(32) Chopdekar, R. V.; Arenholz, E.; Suzuki, Y. Orientation and Thickness Dependence of Magnetization at the Interfaces of Highly Spin-Polarized Manganite Thin Films. *Phys. Rev. B* **2009**, *79*, 104417.

(33) Ott, F.; Viret, M.; Borges, R.; Lyonnet, R.; Jacquet, E.; Fermon, C.; Contour, J.-P. Interface Magnetism of $La_{0.7}Sr_{0.3}MnO_3$ Thin Films Studied by Neutron Reflectometry. *J. Magn. Magn. Mater.* **2000**, *211*, 200−205.

(34) Verna, A.; Davidson, B. A.; Szeto, Y.; Petrov, A. Y.; Mirone, A.; Giglia, A.; Mahne, N.; Nannarone, S. Measuring Magnetic Profiles at

https://dx.doi.org/10.1021/acsami.0c09417
ACS Appl. Mater. Interfaces 2020, 12, 45437−45443

Manganite Surfaces with Monolayer Resolution. *J. Magn. Magn. Mater.* **2010**, *322*, 1212−1216.
(35) Grutter, A. J.; Gilbert, D. A.; Alaan, U. S.; Arenholz, E.; Maranville, B. B.; Borchers, J. A.; Suzuki, Y.; Liu, K.; Kirby, B. J. Reversible Control of Magnetism in $La_{0.67}Sr_{0.33}MnO_3$ through Chemically-Induced Oxygen Migration. *Appl. Phys. Lett.* **2016**, *108*, No. 082405.
(36) Guo, E.-J.; Charlton, T.; Ambaye, H.; Desautels, R. D.; Lee, H. N.; Fitzsimmons, M. R. Orientation Control of Interfacial Magnetism at $La_{0.67}Sr_{0.33}MnO_3/SrTiO_3$ Interfaces. *ACS Appl. Mater. Interfaces* **2017**, *9*, 19307−19312.
(37) Smadici, Ş.; Abbamonte, P.; Bhattacharya, A.; Zhai, X.; Jiang, B.; Rusydi, A.; Eckstein, J. N.; Bader, S. D.; Zuo, J.-M. Electronic Reconstruction at $SrMnO_3$ − $LaMnO_3$ Superlattice Interfaces. *Phys. Rev. Lett.* **2007**, *99*, 196404.
(38) Shannon, R. D.; Prewitt, C. T. Effective Ionic Radii in Oxides and Fluorides. *Acta Crystallogr., Sect. B: Struct. Sci., Cryst. Eng. Mater.* **1969**, *25*, 925−946.
(39) Shannon, R. D. Revised Effective Ionic Radii and Systematic Studies of Interatomic Distances in Halides and Chalcogenides. *Acta Crystallogr., Sect. A: Found. Adv* **1976**, *32*, 751−767.
(40) Zuev, A.; Vylkov, A.; Petrov, A.; Tsvetkov, D. Defect Structure and Defect-Induced Expansion of Undoped Oxygen Deficient Perovskite $LaCoO_{3-\delta}$. *Solid State Ionics* **2008**, *179*, 1876−1879.
(41) Liu, B.; Wang, Y.; Liu, G.; Feng, H.; Yang, H.; Xue, X.; Sun, J. Tuning the Magnetic Properties of $La_{0.67}Sr_{0.33}CoO_{3-\delta}$ Films by Oxygen Pressure. *Phys. Rev. B* **2016**, *93*, No. 094421.
(42) Zuev, A. Y.; Tsvetkov, D. S. Oxygen Nonstoichiometry, Defect Structure and Defect-Induced Expansion of Undoped Perovskite $LaMnO_{3\pm\delta}$. *Solid State Ionics* **2010**, *181*, 557−563.
(43) Kienzle, P. *Neutron Activation and Scattering Calculator*; https://www.ncnr.nist.gov/resources/activation/ (accessed Jun 10, 2019).
(44) Li, B.; Chopdekar, R. V.; Kane, A. M.; Hoke, K.; N'Diaye, A. T.; Arenholz, E.; Takamura, Y. Thickness-Dependent Magnetic and Electrical Transport Properties of Epitaxial $La_{0.7}Sr_{0.3}CoO_3$ Films. *AIP Adv.* **2017**, *7*, No. 045003.
(45) Ji, Y.; Chien, C. L.; Tomioka, Y.; Tokura, Y. Measurement of Spin Polarization of Single Crystals of $La_{0.7}Sr_{0.3}MnO_3$ and $La_{0.6}Sr_{0.4}MnO_3$. *Phys. Rev. B* **2002**, *66*, No. 012410.
(46) Torija, M. A.; Sharma, M.; Gazquez, J.; Varela, M.; He, C.; Schmitt, J.; Borchers, J. A.; Laver, M.; El-Khatib, S.; Leighton, C. Chemically Driven Nanoscopic Magnetic Phase Separation at the $SrTiO_3(001)/La_{1-x}Sr_xCoO_3$ Interface. *Adv. Mater.* **2011**, *23*, 2711−2715.
(47) Hemberger, J.; Krimmel, A.; Kurz, T.; Krug von Nidda, H.-A.; Ivanov, V. Y.; Mukhin, A. A.; Balbashov, A. M.; Loidl, A. Structural, Magnetic, and Electrical Properties of Single-Crystalline $La_{1-x}Sr_xMnO_3$ ($0.4 < x < 0.85$). *Phys. Rev. B* **2002**, *66*, No. 094410.
(48) Sakai, J.; Ito, N.; Imai, S. Oxygen Content of $La_{1-x}Sr_xMnO_{3-y}$ Thin Films and Its Relation to Electric-Magnetic Properties. *J. Appl. Phys.* **2006**, *99*, No. 08Q318.
(49) Urushibara, A.; Moritomo, Y.; Arima, T.; Asamitsu, A.; Kido, G.; Tokura, Y. Insulator-Metal Transition and Giant Magnetoresistance in $La_{1-x}Sr_xMnO_3$. *Phys. Rev. B* **1995**, *51*, 14103−14109.
(50) Gazquez, J.; Bose, S.; Sharma, M.; Torija, M. A.; Pennycook, S. J.; Leighton, C.; Varela, M. Lattice Mismatch Accommodation via Oxygen Vacancy Ordering in Epitaxial $La_{0.5}Sr_{0.5}CoO_{3-\delta}$ Thin Films. *APL Mater.* **2013**, *1*, No. 012105.

https://dx.doi.org/10.1021/acsami.0c09417
ACS Appl. Mater. Interfaces 2020, 12, 45437−45443